npj | Quantum Materials

www.nature.com/npjquantmats

ARTICLE OPEN

Check for updates

Metal–insulator-like transition, superconducting dome and topological electronic structure in Ga-doped Re_3Ge_7

Yanwei Cui[1,2,3,5], Siqi Wu[3,5], Qinqing Zhu[1,2,4], Guorui Xiao[1,2,3], Bin Liu[1,2,4], Jifeng Wu[1,2,4], Guanghan Cao[3] and Zhi Ren[1,2]✉

Superconductivity frequently appears by doping compounds that show a collective phase transition. So far, however, this has not been observed in topological materials. Here we report the discovery of superconductivity induced by Ga doping in orthorhombic Re_3Ge_7, which undergoes a second-order metal–insulator-like transition at ~58 K and is predicted to have a nontrivial band topology. It is found that the substitution of Ga for Ge leads to hole doping in $Re_3Ge_{7-x}Ga_x$. As a consequence, the phase transition is gradually suppressed and disappears above $x = 0.2$. At this x value, superconductivity emerges and T_c exhibits a dome-like doping dependence with a maximum value of 3.37 K at $x = 0.25$. First principles calculations suggest that the phase transition in Re_3Ge_7 is associated with an electronic instability driven by Fermi-surface nesting and the nontrival band topology is preserved after Ga doping. Our results indicate that Ga-doped Re_3Ge_7 provides a rare opportunity to study the interplay between superconductivity and competing electronic states in a topologically nontrivial system.

npj Quantum Materials (2021)6:74 ; https://doi.org/10.1038/s41535-021-00372-z

INTRODUCTION

The emergence of superconductivity (SC) in the vicinity of a competing electronic state has received great attention over the past few decades. Well-known examples include cuprates[1], heavy fermions[2], transition metal chalcogenides[3], and iron pnictides[4]. Their parent compounds exhibit either an antiferromagnetic[5–7] or a charge-density-wave (CDW) transition[8], which is sometimes accompanied by a change from metallic to nonmetallic behavior[9,10]. Understanding the interplay between these transitions and SC not only sheds light on the pairing mechanism, but also provides an effective route for the search of new superconductors. Recently, the topological aspects of superconductors have become a focus of interest[11–13]. These topological superconductors (TSCs) have a bulk superconducting gap but host gapless edge states consisting of Majorana fermions. Many proposals to create TSCs have been put forward and a significant progress has been made. In particular, chemical doping of topological materials is shown to be one of the most promising ways for this purpose[14–20]. However, in all known cases, there exit no competing ground state in the parent compounds.

Re_3Ge_7 is the only binary phase in the Re-Ge system and crystallizes in the orthorhombic structure with the *Cmcm* space group[21], which is sketched in Fig. 1a, b. Its structure can be viewed as consisting of isolated Re_3B-type $ReGe_3$ and double $NbAs_2$-type Re_2Ge_4 prisms[21]. Although Re_3Ge_7 has been known to exist for nearly 40 years, its thermodynamic and transport properties are reported only very recently[22]. The results indicate that the compound is weakly diamagnetic while undergoes a second-order phase transition below 58.5 K as confirmed by specific-heat measurements. This transition is accompanied by a drop in the diamagnetic susceptibility, a metal-to-insulator-like transition in resistivity, and a strong reduction in electron carrier concentration. While it is suspected that the phase transition in Re_3Ge_7 has a structural origin, no low-temperature X-ray study has been performed. On the other hand, theoretical calculations suggest that Re_3Ge_7 is a high-symmetry point topological semimetal[23]. Since the combination of these properties in a single material is uncommon, it is of significant interest to see what would be the ground state once the phase transition is suppressed.

Here we show that, upon hole doping by substituting Ge with Ga, Re_3Ge_7 turns into a bulk superconductor. The resulting temperature-doping phase diagram for $Re_3Ge_{7-x}Ga_x$ resembles closely those of the correlated electron systems. Especially, as the metal–insulator transition is suppressed continuously and disappears completely for $x > 0.2$, a dome-like superconducting phase is observed for x between 0.2 and 0.4 with a maximum T_c of 3.37 K at $x = 0.25$. The effect of Ga doping on the electronic band structure and topology in Re_3Ge_7 is investigated by first principles calculations, and the implication of these results is discussed.

RESULTS AND DISCUSSION

Structural characterization

The X-ray diffraction (XRD) results for the series of $Re_3Ge_{7-x}Ga_x$ samples at room temperature are displayed in Fig. 1c. The patterns are very similar and all the diffraction peaks can be well indexed on the basis of an orthorhombic unit-cell with the *Cmcm* space group. The refined lattice parameters as well as the unit-cell volume V are plotted as a function of the Ga content x in Fig. 1d–g. For undoped Re_3Ge_7 ($x = 0$), the *a*-, *b*-, and *c*-axis lattice constants are found to be 3.227(1) Å, 9.044(1) Å, and 21.960(1) Å, respectively, which are in excellent agreement with the previous report[21]. With increasing x, both *a*- and *b*-axis expand, which is as expected since since the atomic radius of Ga (1.388 Å) is larger than that of Ge (1.349 Å)[24]. Nevertheless, the *c*-axis shrinks more rapidly, which leads to a small contraction of the unit-cell volume (up to ~0.2%).

In Re_3Ge_7, Re atoms occupy two different crystallographic sites (0, 0.074, 0.559) and (0, 0.48, 0.25), and there are four distinct sites

[1]Key Laboratory for Quantum Materials of Zhejiang Province, School of Science, Westlake University, Hangzhou, PR China. [2]Institute of Natural Sciences, Westlake Institute for Advanced Study, Hangzhou, PR China. [3]Department of Physics, Zhejiang University, Hangzhou, PR China. [4]Department of Physics, Fudan University, Shanghai, PR China. [5]These authors contributed equally: Yanwei Cui, Siqi Wu. ✉email: renzhi@westlake.edu.cn

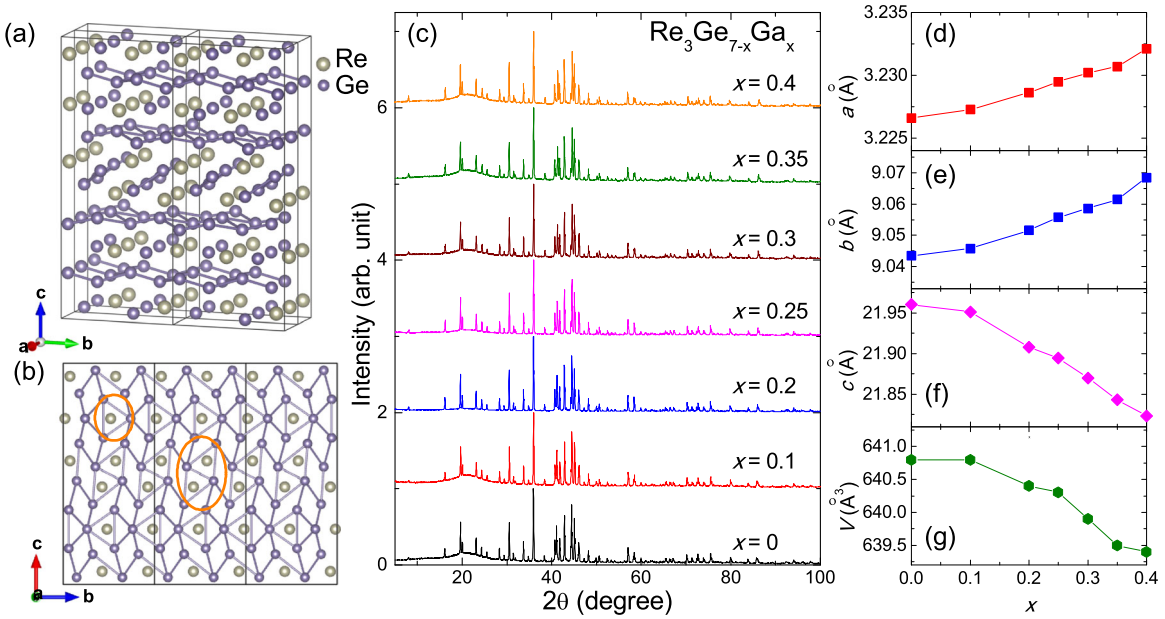

Fig. 1 Schematic crystal structure and x-ray diffraction results of $Re_3Ge_{7-x}Ga_x$. a A three-dimensional view of the orthorhombic structure of Re_3Ge_7. **b** Structure of Re_3Ge_7 projected perpendicular to the *a*-axis. The circles indicate the $ReGe_3$ and Re_2Ge_4 building blocks. **c** Room temperature powder XRD patterns for the series of $Re_3Ge_{7-x}Ga_x$ samples. **d–g** Variation of *a*-, *b*-, *c*-axis lattice parameters and unit-cell volume of $Re_3Ge_{7-x}Ga_x$ as a function of the Ga content *x*.

for Ge: (0, 0.061, 0.163), (0, 0.324, 0.137), (0, 0.353, 0.532), and (0, 0.761, 0.25). For the structural refinements of $Re_3Ge_{7-x}Ga_x$, the Ga atoms are assumed to be distributed randomly on the four Ge sites (see Table 1). Representative refinement results in the 2θ region near the strongest peak for $x = 0$, 0.2, and 0.4 are shown in Fig. 2a–c (results for full patterns are shown in Supplementary Fig. 1). In all cases, the calculated XRD patterns match well with the observed ones, which is corroborated by the small R_{wp} (4.4–5.9%) and R_p (3.2–4.3%) factors. Hence all samples are free of discernible impurities, confirming their high quality. In passing, we have also performed low-temperature XRD measurements on Re_3Ge_7 down to 15 K. The data reveal that the lattice parameters vary smoothly with decreasing temperature and there is no evidence for a structural transition (see Supplementary Fig. 2).

Table 1. Atomic coordinates for $Re_3Ge_{7-x}Ga_x$.

Atoms	site	*x*	*y*	*z*	Occupancy
Re (1)	8*f*	0	0.074	0.559	1
Re (2)	4*c*	0	0.48	0.25	1
Ge (1)/Ga (1)	8*f*	0	0.061	0.163	(7−*x*)/*x*
Ge (2)/Ga(2)	8*f*	0	0.324	0.137	(7−*x*)/*x*
Ge (3)/Ga (3)	8*f*	0	0.353	0.532	(7−*x*)/*x*
Ge (4)/Ga (4)	4*c*	0	0.761	0.25	(7−*x*)/*x*

Suppression of the metal–insulator-like transition

A systematic change in the resistivity (ρ) of $Re_3Ge_{7-x}Ga_x$ is observed with increasing *x*, which is shown in Fig. 3a. On cooling below room temperature, the pristine Re_3Ge_7 exhibits a metallic behavior but undergoes a metal–insulator transition below $T_{MI} =$ 57.3 K. At 1.8 K, the residual resistivity ratio (RRR) is much smaller than unity. This overall behavior is well consistent with that observed in single-crystal samples[22]. When Ga is introduced into the system, the ρ at high temperature increases monotonically and the metal–insulator transition is gradually suppressed. Actually, the ρ value at 1.8 K for $x = 0.1$ is only about half that for $x = 0$. In addition, the application of magnetic field has little effect on the T_{MI} while results in a positive magnetoresistance at low temperature (data not shown). As *x* increases above 0.2, T_{MI} can no longer be resolved and RRR becomes significantly larger than one with a maximum value of 7.4 at $x = 0.25$, signifying a good metallic behavior.

The doping evolution of temperature-dependent magnetic susceptibility $\chi(T)$ measured under a field of 7 T for $Re_3Ge_{7-x}Ga_x$ is displayed in Fig. 3b. All the $\chi(T)$ data are negative and nearly temperature independent, substantiating that the magnetic properties of these samples are dominated by the core diamagnetism. With increasing *x*, however, the $\chi(T)$ data become less negative, and hence the Pauli paramagnetic contribution seems to grow with the Ga content. This trend implies an enhancement of the density of states at the Fermi level [$N(E_F)$] induced by Ga doping, consistent with the results shown below. For $x \le 0.2$, a drop in $\chi(T)$ is detected and its magnitude decreases as the increase of *x*. Note that the onset temperature of this anomaly agrees with T_{MI} determined from resistivity measurements (see the dashed line). Across the metal–insulator-like transition, it is reasonable to speculate that a gap opens at the Fermi level and hence $N(E_F)$ decreases[3]. Since the Pauli paramagentic susceptibility is proportional to $N(E_F)$, this leads to a decrease in χ as observed experimentally. At low temperature, the $\chi(T)$ data exhibit a weak upturn, which is ascribed to a small amount of paramagnetic impurities.At low temperature, the $\chi(T)$ data exhibit a weak upturn, which is ascribed to a small amount of paramagnetic impurities.

The specific heats C_p of $Re_3Ge_{7-x}Ga_x$ are also measured and shown in Fig. 3c. The data for all *x* values almost overlap with each other. In addition, the C_p values at high temperatures are close to the Dulong–Petit limit of $3NR = 249.92$ J mol^{-1} K^{-1}, where $N = 10$ and $R = 8.314$ J mol^{-1} K^{-1} is the molar gas constant. On close examination, a C_p anomaly is found near 57 K for $x = 0$ and 0.1 (see the inset), confirming that the metal–insulator transition is of second order. At higher *x* values, no such anomaly is discernible, suggesting that the transition is either too weak to be detected or completely suppressed.

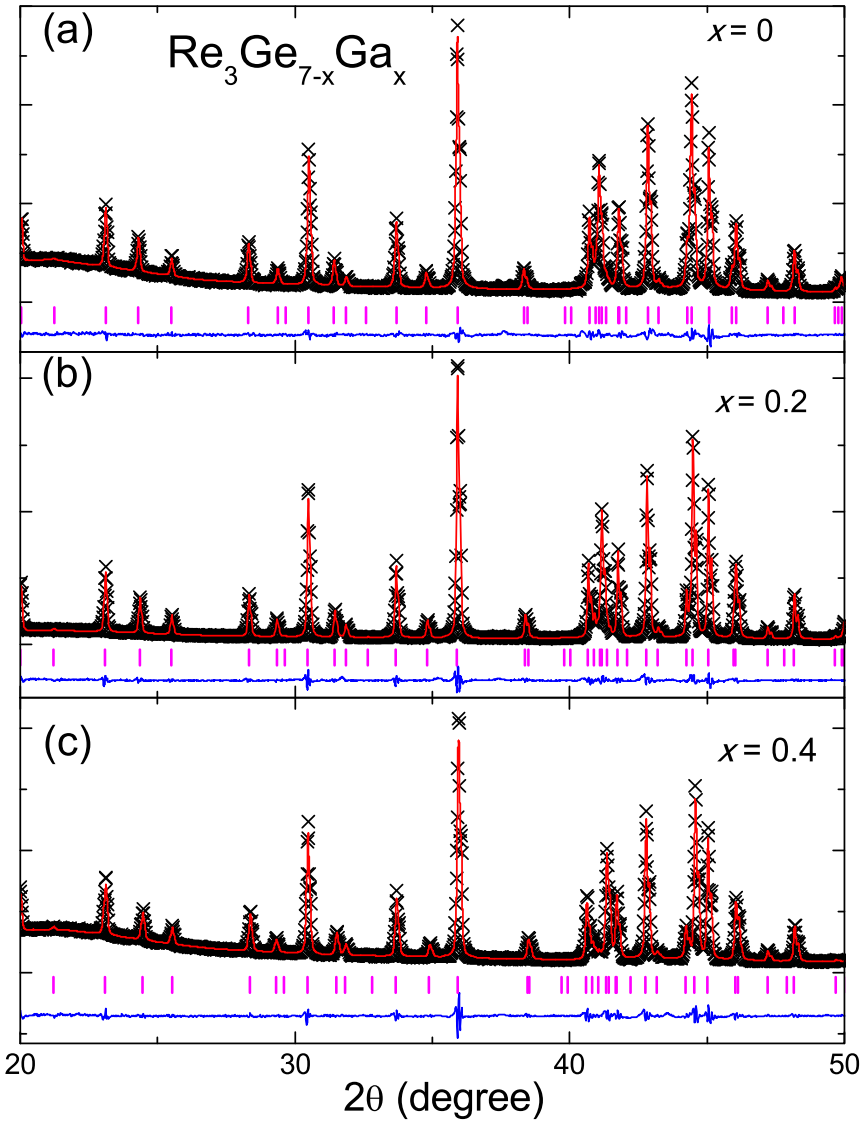

Fig. 2 Structural refinement of $Re_3Ge_{7-x}Ga_x$. a–c Structural refinement profiles in the 2θ range of 20 to 50° for the $Re_3Ge_{7-x}Ga_x$ samples with $x = 0$, 0.2, and 0.4, respectively.

The effect of Ga doping on the carrier concentration of $Re_3Ge_{7-x}Ga_x$ is further investigated by the Hall effect measurements. Figure 3d, e shows the magnetic field dependence of Hall resistivity ρ_H for two cases of $x = 0$ and 0.25, which show clear contrast. In the former case, the ρ_H data are negative above 50 K, but become positive at lower temperatures. This indicate the presence of both hole and electron carriers in the system, which naturally explains the nonlinear ρ_H as a function of magnetic field. In the latter case, however, ρ_H is positive and depends linearly on the field. The temperature dependence of Hall coefficient R_H for the series of samples shown in Fig. 3f. Here R_H is determined as $R_H = \rho_H/B$ in the low-field region. With decreasing temperature, R_H for $x = 0$ and 0.1 undergoes a sign reversal from negative to positive, and then rises steeply before reaching a plateau. Note that the sign-reversal temperature is close to T_{MI}, suggesting that the two phenomena are intimately related. At higher x values, R_H is always positive and no sign-reversal occurs. Nevertheless, a rise in R_H is still observable below a temperature around T_{MI} for $x = 0.2$. Remarkably, the low-temperature R_H values for $x \le 0.1$ are about two-orders magnitude higher than those for $x \ge 0.25$. This implies that the latter has a much higher hole concentration, which is estimated to be ~1.2–2 × 10^{21} cm^{-3} assuming a one-band model. These results demonstrate that Ga doping introduces holes in Re_3Ge_7. Nonetheless, given the orthorhombic structure and multiband nature of $Re_3Ge_{7-x}Ga_x$, Hall measurements on single crystals are needed to determine more precisely the evolution of carrier concentration with varying Ga content.

Emergence of superconductivity

As a consequence of this doping, SC is induced in $Re_3Ge_{7-x}Ga_x$ over an x range of 0.2–0.4. This is demonstrated by the $\rho(T)$ and $\chi(T)$ data below 4 K in Fig. 4a, b. As can be seen in Fig. 4a, a drop to zero resistivity is observed for all x values in this range. With increasing x, the resistive transition first shifts to higher temperatures and then to lower temperatures, displaying a non-monotonic behavior. The T_c values, determined from the midpoints of the ρ drops, are 1.81, 3.37, 2.56, 2.08, and 1.49 K for $x = 0.2$, 0.25, 0.3, 0.35, and 0.4, respectively. Meanwhile, the zero-field cooling susceptibility χ_{ZFC} of these samples measured under 1 mT exhibits a strong diamagnetic response, whose onset temperature coincides with T_c. In addition, their shielding factions are estimated to exceed ~150% without demagnetization correction.

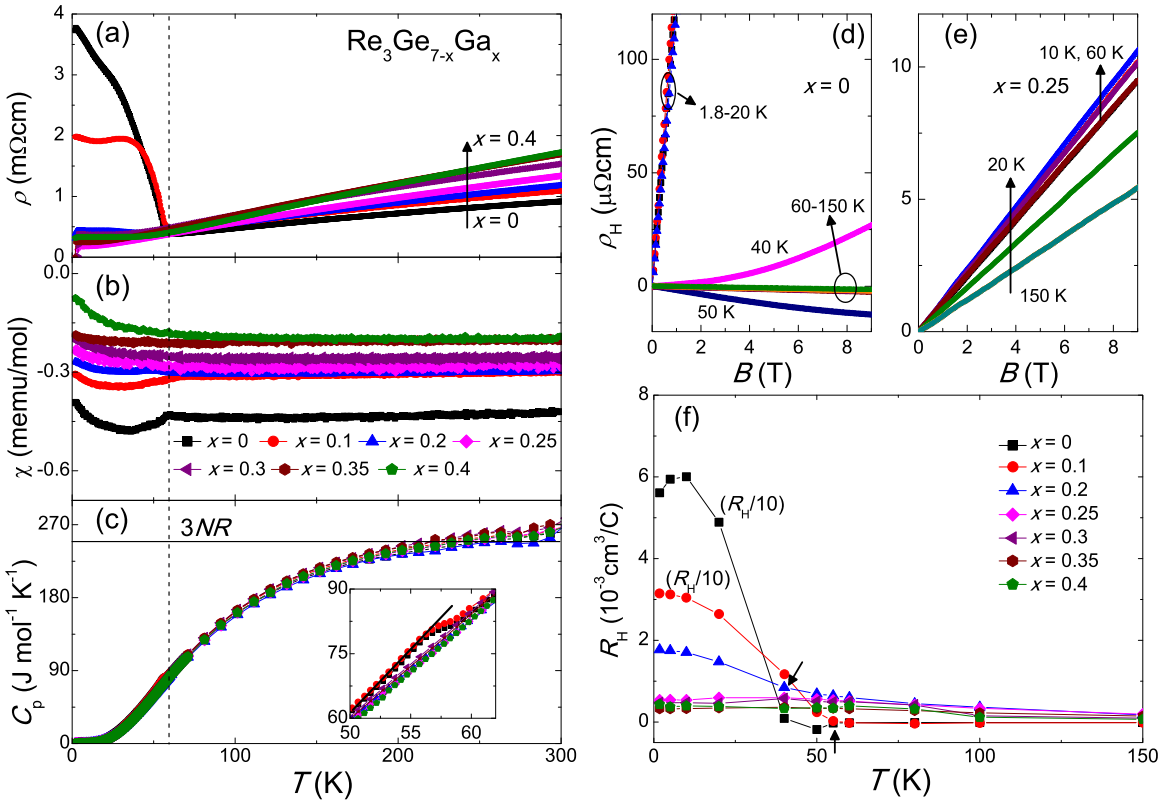

Fig. 3 Evolution of resistivity, magnetic susceptibility, specific-heat, and Hall coefficient with Ga content in $Re_3Ge_{7-x}Ga_x$. a–c Temperature dependence of resistivity, magnetic susceptibility, and specific heat below 300 K for the series of $Re_3Ge_{7-x}Ga_x$ samples, respectively. The vertical dashed line is a guide to the eyes. In (**a**), the arrow marks the increasing of Ga content *x*. In (**c**), the horizontal line is the Dulong–Petit limit of $3NR = 249.42\ J\ mol^{-1}\ K^{-1}$, and the inset shows a zoom of the data between 50 and 62 K. **d**, **e** Magnetic field dependence of Hall resistivity at various temperatures for the samples with $x = 0$ and 0.2, respectively. The circles and arrows are a guide to the eyes. **f** Temperature dependence of Hall coefficient for the series of samples. The anomalies are marked by the arrows, and the data for both $x = 0$ and 0.1 are divided by a factor of 10 for better illustration.

The bulk nature of SC is confirmed by the plots of low-temperature C_p/T versus T^2 in Fig. 4c. A clear C_p jump is observed for the *x* value of 0.25, 0.3 and 0.35. As for $x = 0.2$ and 0.4, the absence of such an anomaly is due to that their T_c values are below the lowest measurement temperature (1.8 K). On the other hand, the normal-state C_p data for both undoped and Ga-doped Re_3Ge_7 are well fitted by the Debye model

$$C_p/T = \gamma + \beta T^2 + \delta T^4, \quad (1)$$

where γ and $\beta(\delta)$ are the electronic and phonon specific-heat coefficients, respectively. From β, the Debye temperature Θ_D is calculated as

$$\Theta_D = \left(\frac{12\pi^4 NR}{5\beta}\right)^{1/3}. \quad (2)$$

The obtained γ and Θ_D are listed in Table 2. Intriguingly, while no systematics in Θ_D are observed, γ exhibits a nonmonotontic *x* dependence with a maximum value of 13.6 mJ $mol^{-1}\ K^{-2}$ at $x = 0.25$. This value is larger than those of the conventional metals[25] and comparable to those of some iron-based superconductors with a similar carrier concentration[26].

It is prudent to note that the γ value (=2.5 mJ $mol^{-1}\ K^{-2}$) of our polycrystalline Re_3Ge_7 sample is much larger than that (~4 μJ $mol^{-1}\ K^{-2}$) of the single crystalline one[22]. Moreover, the signs of their R_H data at low temperature are opposite. These contrasts are most probably due to slight difference in stoichiometry of the two samples. As a matter of fact, we have also grown Re_3Ge_7 crystals with (00*l*) orientation using a flux method different from that in ref. [22], where crystals with (0*l*0) orientation were obtained. The Hall measurements indicate that its R_H is positive in the whole temperature range (data not shown). It is thus possible that the sign of R_H depends on the crystal orientations. Since our polycrystalline samples consist of many small crystals with random orientations, it is no wonder that the sign of R_H is different from that measured on single crystals.

The normalized electronic specific-heat $C_{el}/\gamma T$ for $0.25 \le x \le 0.35$, obtained by subtraction of the phonon contribution, is shown in Fig. 4d. It turns out that the $C_{el}/\gamma T$ jump decreases with increasing *x* and hence increasing T_c. Using an entropy conserving construction, $\Delta C_{el}/\gamma T$ is determined to be 0.83 and 1.08 for $x = 0.25$ and 0.3, respectively, which are significantly smaller than the BCS value of 1.43[27]. Indeed, the temperature dependence of their $C_{el}/\gamma T$ data show a clear deviation from the weak coupling BCS theory[27], hinting at the presence of multiple superconducting gaps or even gap nodes. Hence, to better understand the gap structure, C_p measurements at temperatures much below T_c are needed. Nevertheless, since inhomogeneity could be present is our polycrystalline samples, such investigation is best performed on single crystals and thus left for future studies.

The upper critical fields B_{c2} for $Re_3Ge_{7-x}Ga_x$ with $0.25 \le x \le 0.35$ are determined by resistivity measurements under magnetic fields. An example for $x = 0.25$ is shown in Fig. 4e. As expected, the resistive superconducting transition shifts toward lower temperatures and becomes broadened as the field increases. At each field, the T_c value is determined using the same criterion as above. The resulting B_{c2} versus temperature phase diagrams are displayed in Fig. 4f. All the $B_{c2}(T)$ data are well described by the

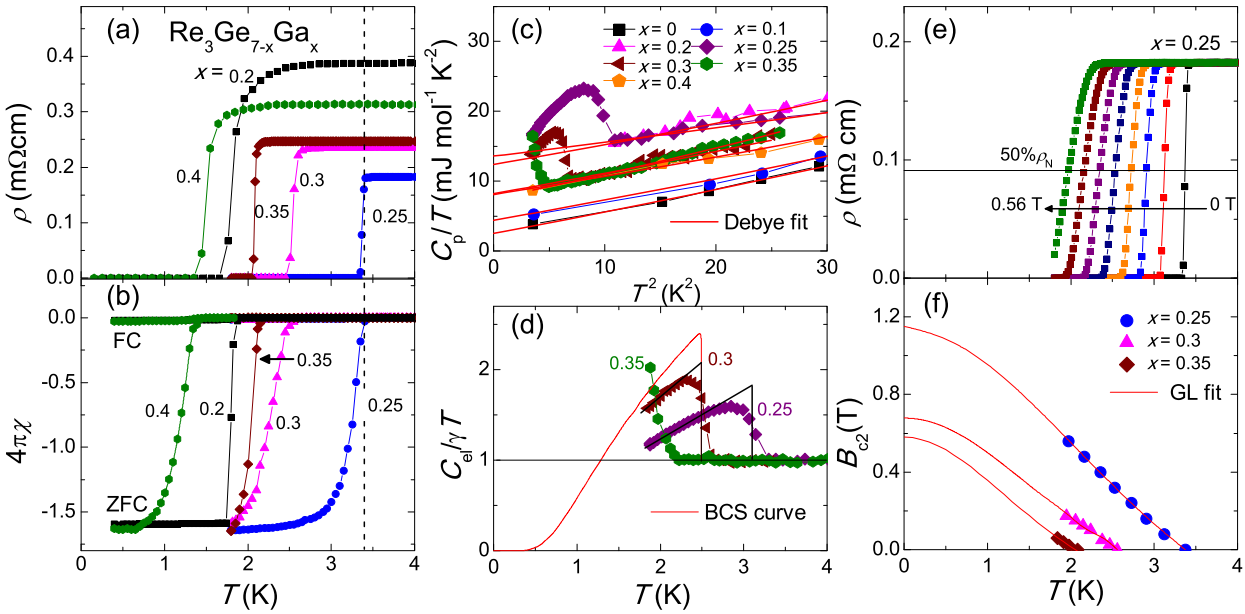

Fig. 4 Superconducting transition and upper critical field of $Re_3Ge_{7-x}Ga_x$. **a**, **b** Low-temperature resistivity and magnetic susceptibility for $Re_3Ge_{7-x}Ga_x$ with $0.2 \le x \le 0.4$, respectively. The vertical dashed line is a guide to the eyes. **c** Low-temperature specific-heat C_p data for all the $Re_3Ge_{7-x}Ga_x$ samples plotted as C_p/T versus T^2. The solid lines are fits by the Debye model. **d** Temperature dependence of normalized electronic specific-heat for the samples with $0.25 \le x \le 0.35$. The back lines are energy conserving constructions to estimate the specific-heat jump and the red line denotes the theoretical BCS curve. **e** Temperature dependence of resistivity under various fields up to 0.56 T for the sample with $x = 0.2$, and the field increment is 0.08 T. The horizontal line and arrow indicate the 50% drop of normal-state resistivity and field increasing direction, respectively. **f** Upper critical field versus temperature phase diagram for the samples with $0.25 \le x \le 0.35$. The solid lines are fits to the data by the Ginzburg–Landau model.

Table 2. Structural refinement results and physical parameters of $Re_3Ge_{7-x}Ga_x$.

Parameter	$x = 0$	$x = 0.1$	$x = 0.2$	$x = 0.25$	$x = 0.3$	$x = 0.35$	$x = 0.4$
a (Å)	3.226 (1)	3.227 (1)	3.228 (1)	3.229 (1)	3.230 (1)	3.231 (1)	3.232 (1)
b (Å)	9.044 (1)	9.046 (1)	9.052 (1)	9.056 (1)	9.059 (1)	9.062 (1)	9.068 (1)
c (Å)	21.960 (1)	21.951 (1)	21.908 (1)	21.895 (1)	21.870 (1)	21.843 (1)	21.823 (1)
R_{wp}	5.0%	5.5%	7.5%	6.0%	5.9%	4.5%	4.6%
R_p	3.7%	4.0%	5.3%	4.4%	4.4%	3.3%	3.4%
T_{MI} (K)	57.3	53.4	47.7	–	–	–	–
T_c (K)	–	–	1.81	3.37	2.56	2.08	1.49
γ (mJ mol^{-1} K^{-2})	2.5	4.4	12.4	13.6	8.2	7.5	8.1
Θ_D (K)	402	411	416	468	411	389	427
B_{c2} (0) (T)	–	–	–	1.15	0.68	0.58	–
ξ_{GL} (nm)	–	–	–	16.9	22.0	23.8	–

Ginzburg–Landau (GL) model

$$B_{c2}(T) = B_{c2}(0)\frac{1 - t^2}{1 + t^2}, \quad (3)$$

where $B_{c2}(0)$ is the zero-temperature upper critical field and $t = T/T_c$. The obtained $B_{c2}(0)$ is 1.15 T for $x = 0.25$, 0.68 T for $x = 0.3$, and 0.58 T for $x = 0.35$. Once $B_{c2}(0)$ is known, the GL coherence length ξ_{GL} can be calculated by the equation

$$\xi_{GL} = \sqrt{\frac{\Phi_0}{2\pi B_{c2}(0)}}, \quad (4)$$

where $\Phi_0 = 2.07 \times 10^{-15}$ Wb is the flux quantum. This gives ξ_{GL} values of 16.9, 22.0, and 23.8 nm for $x = 0.25$, 0.3, and 0.35, respectively.

Electronic phase diagram

The above results, which are also summarized in Table 2, allow us to construct the electronic phase diagram of $Re_3Ge_{7-x}Ga_x$ presented in Fig. 5a. Upon Ga doping, T_{MI} in Re_3Ge_7 is gradually suppressed and disappears abruptly at $x > 0.2$. Note that, below T_{MI}, the carrier concentration decreases by more than one order of magnitude as indicated by the above Hall measurements. This drastic variation is closely related to the second-order phase transition and hence differs from the case of a semimetal with a small pocket. Instead, the negative temperature coefficient of resistivity ($d\rho/dT < 0$) below T_{MI} is reminiscent of an insulating-like behavior, as we labeled in the phase diagram. On the other hand, SC emerges for $x \ge 0.2$, and T_c shows a dome-like dependence on x with a maximum of 3.37 K observed at $x = 0.25$. The contrasting behavior of T_{MI} and T_c suggests that there is a competition between the insulating-like and superconducting phases, though

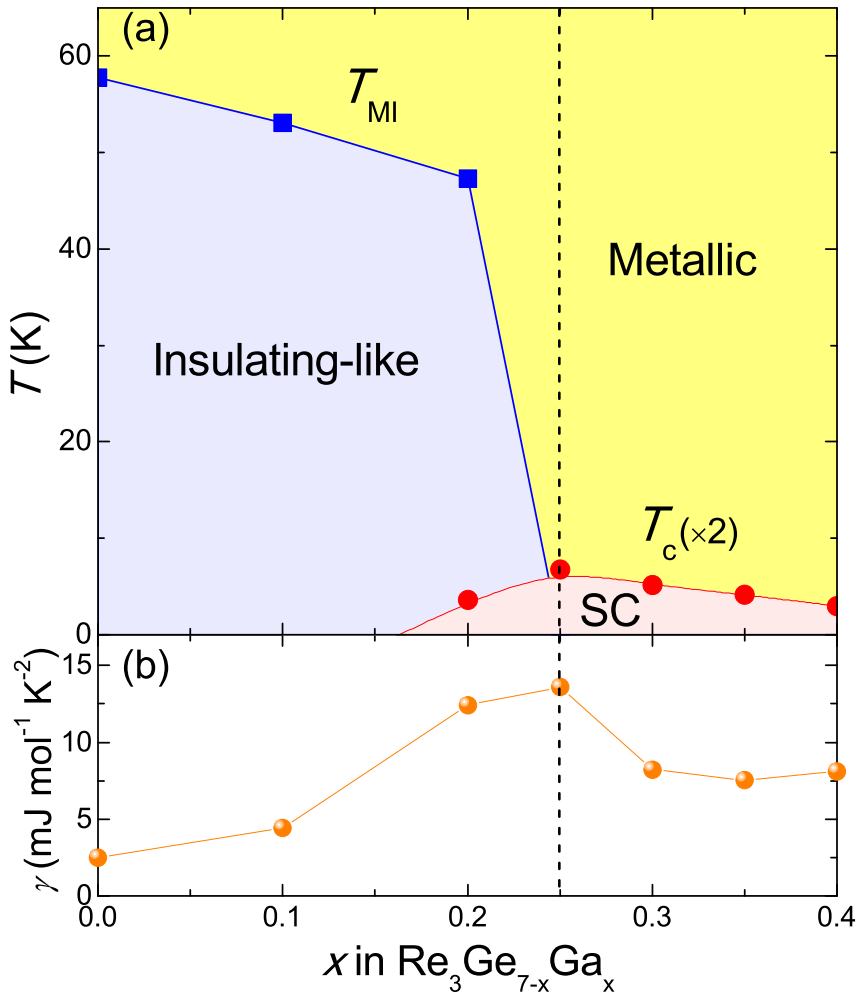

Fig. 5 Electronic phase diagram of $Re_3Ge_{7-x}Ga_x$ and its comparison with the variation of electronic specific heat. a *T-x* electronic phase diagram of $Re_3Ge_{7-x}Ga_x$. Note that the T_c data are multiplied by a factor of 2 for clarity. **b** *x* dependence of electronic specific-heat coefficient, respectively. The vertical dashed line is a guide to the eyes.

the two phases might coexist in a narrow *x* range between 0.2 and 0.25. Moreover, the maximum in T_c coincides well with that of γ, suggesting that the enhanced density of states (DOS) may play an important role in the superconducting pairing. It should be pointed out, for each *x* value, we have carried out measurements on multiple samples. An example of $x = 0.25$ and data summary are shown in Supplementary Fig. 3 and Table 1, respectively. These results indicate that the error bar in characteristic temperatures is within the symbol size, and hence the overall phase diagram is well reproducible.

Calculated band structure

To gain insight into the effect of Ga doping in Re_3Ge_7, we performed first principles calculations on the electronic structure of $Re_3Ge_{7-x}Ga_x$ with *x* up to 0.4. The calculated band dispersions with and without spin–orbit coupling (SOC) are shown in Fig. 6a, and the Brillouin zone is sketched in Fig. 6b. One can see that there are several bands crossing E_F and the Ga doping mainly leads to a rigid band shift of the Fermi level (E_F) (see Supplementary Fig. 4). Without considering SOC, there are three fourfold degenerate points about 0.3 eV above E_F along the X-R line. Nevertheless, when turning on SOC, only the one located at R point remains ungapped. Group theory analysis of the $\mathbf{k}\cdot\mathbf{p}$ perturbation matrix elements shows that the energy bands around this fourfold point have linear dispersions[28], which is protected by the nonsymmorphic space group *Cmcm*. Since R is a time-reversal invariant momentum, the linear dispersions for Kramers partners must be reversed. Thus despite that the band dispersion is tilted, the fourfold point at R is a type-I Dirac point[29], in agreement with the previous report[23].

Figure 6c–h shows the calculated Fermi-surface and its nesting function along the high-symmetry lines for $Re_3Ge_{7-x}Ga_x$. For undoped Re_3Ge_7 ($x = 0$), its Fermi surface consists of two large hole pockets along the $\mathbf{k}_y$ direction and two sets of small electron pockets crossing the G-X and Y-X1 lines. Upon Ga doping, the hole pockets remain nearly unchanged while the electron pockets become smaller and vanish for $x \geq 0.1$. These results are well consistent with the evolution of R_H data and confirm Ga as a hole dopant. Nevertheless, since the metal–insulator-like transition is not considered in the calculation, a direct comparison between the evolutions of theoretical DOS and experimental γ values with Ga content is not meaningful. On the other hand, the nesting function exhibits peaks around X, X1, Z points, and along G-X, G-Y-X1 lines, in addition to the universal one at Γ point. Nevertheless, only the peaks along G-X and Y-X1 lines (marked by $\mathbf{q}_1$ and $\mathbf{q}_2$ in Fig. 6h) are significantly suppressed with Ga doping, while the other peaks survive at higher doping level. The corresponding wave vectors for these peaks are $\mathbf{q}_1 = (\pm 0.06, 0, 0)$ and $\mathbf{q}_2 = (\pm 0.02, 1, 0)$ in the unit of $(\pi/a, \pi/b, \pi/c)$. By careful inspection of the Fermi-surface structure, we find that the nesting peaks at $\mathbf{q}_1$ and $\mathbf{q}_2$ are closely related to the electron pockets, as shown in Fig. 6i. The $\mathbf{q}_1$

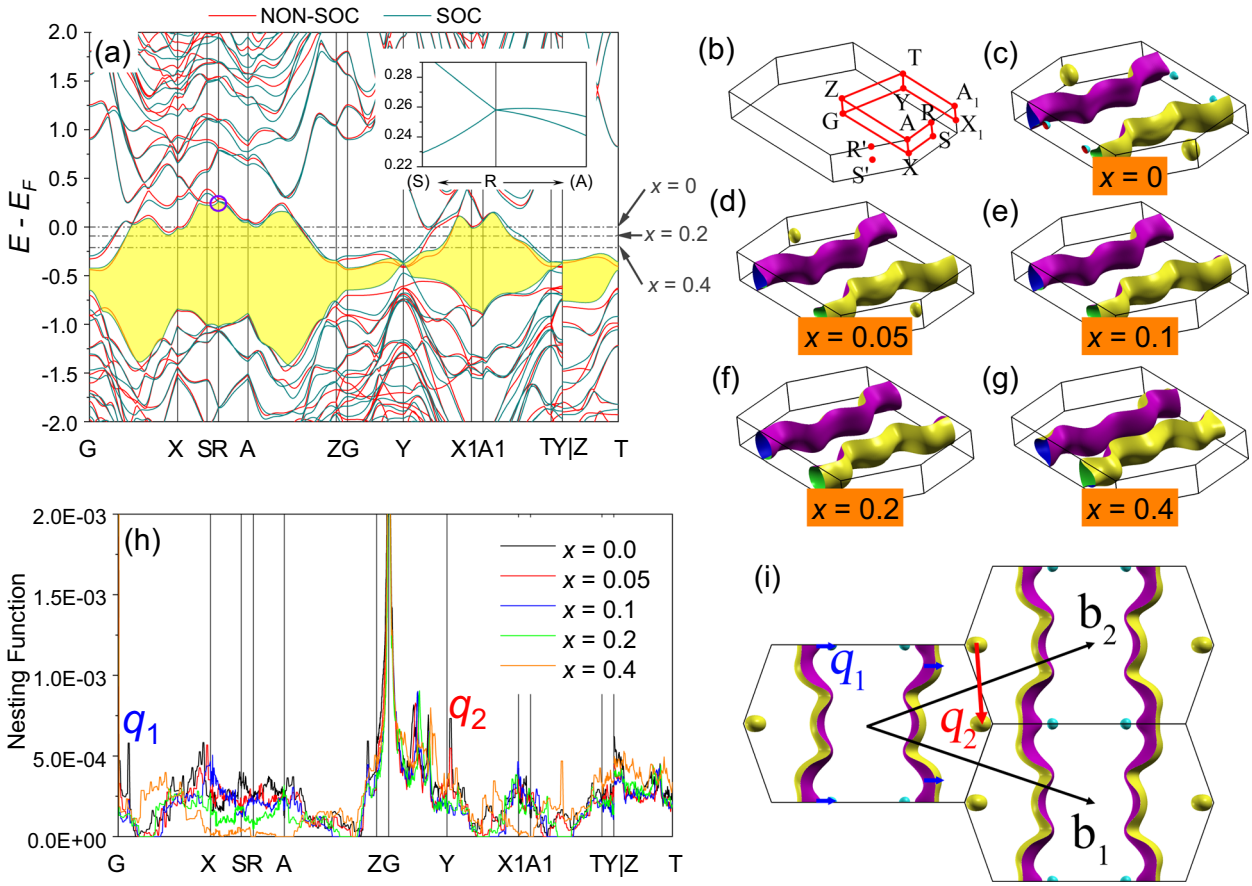

Fig. 6 Calculated electronic structure and Fermi-surface nesting functions of $Re_3Ge_{7-x}Ga_x$. **a** Bulk band structure for $Re_3Ge_{7-x}Ga_x$ without and with SOC. The yellow shaded region corresponds to the band filling of $x = 1$. **b** Brillouin zone of $Re_3Ge_{7-x}Ga_x$ with high-symmetry points and lines. **c**–**g** The Fermi-surface for $Re_3Ge_{7-x}Ga_x$ with $x = 0$, 0.05, 0.1, 0.2, and 0.4, respectively. **h** The calculated Fermi-surface nesting functions at high-symmetry lines. **i** A diagrammatic sketch of nesting vectors $\mathbf{q}_1$ and $\mathbf{q}_2$.

peak should be mainly contributed by the nesting between the hole and electron pockets. Nevertheless, since trace of $\mathbf{q}_1$ is still present at higher Ga doping levels, it is reasonable to infer that this peak is also contributed by the nesting between the hole pockets. For the peak of $\mathbf{q}_2$, it disappears as soon as the electron pockets vanish and thus should result from the nesting between the ellipsoid-shaped electron pockets around X point. This is corroborated by the 2D nesting functions shown in Supplementary Fig. 5. It is noted that the metal–insulator-like transition and the above-mentioned nesting peaks are suppressed at almost the same Ga doping level. It is therefore reasonable to speculate that the phase transition in pristine Re_3Ge_7 is associated with a nesting driven Fermi-surface instability[30,31].

Nontrivial band topology

Now let's examine the band topology of $Re_3Ge_{7-x}Ga_x$. As illustrated in Fig. 6a, a moderate doping of $x = 1$ would lower the electron filling level into the yellow full-gapped region. Given that Re_3Ge_7 holds the spatial inversion symmetry, one can obtain the Z_2 invariants by calculating the inversion parities[32,33]. This gives Z_2 invariants of (1;110), which corresponds to a strong topological insulator (TI) phase. Since the Dirac point is protected by the nonsymmorphic space group, it is of interest to investigate the configuration that breaks the nonsymmorphic group symmetry. In Fig. 7a, we present a hypothetical structure of Re_3Ge_6Ga, which is derived by replacing 2 Ge atoms of Ge(1) site with Ga (per primitive cell). Such a configuration lowers the symmetry group to *C*2/*m*, which has only 2-dimensional double valued irreducible representations. Thus one expect that the bands are doubly degenerated at any high-symmetry points, which split the Dirac point into two doubly degenerated points. The calculated band structure for Re_3Ge_6Ga is shown in Fig. 7b. Indeed, the Dirac point at R point splits into a full-gapped region (the cyan shaded region), while the yellow shaded region remains gapped. The Z_2 invariants are calculated to be (0;001) and (1;110) for the cyan and yellow regions, respectively. This not only demonstrates the robustness of the strong TI phase in Ga-doped Re_3Ge_7, but also indicates that Re_3Ge_7 will become a weak TI by breaking the nonsymmorphic group symmetry.

Perspective and summary

Finally, we discuss the implications of our results and suggest some directions for future research. First, since the overall properties of $Re_3Ge_{7-x}Ga_x$ are similar to those of Cu_xTiSe_2[3], the phase transition in Re_3Ge_7 could be due to the CDW formation, which calls for verification by temperature-dependent electron diffraction studies. Second, the emergence of SC by only ~3% Ga doping implies that Re_3Ge_7 lies on the verge of a superconducting instability. It is therefore of interest to see whether SC can be induced by doping with other elements or the application of high pressure. Third, the combination of SC and nontrivial band topology renders $Re_3Ge_{7-x}Ga_x$ a potential candidate for TSC[11–13]. In this respect, single-crystal growth is highly desirable for further

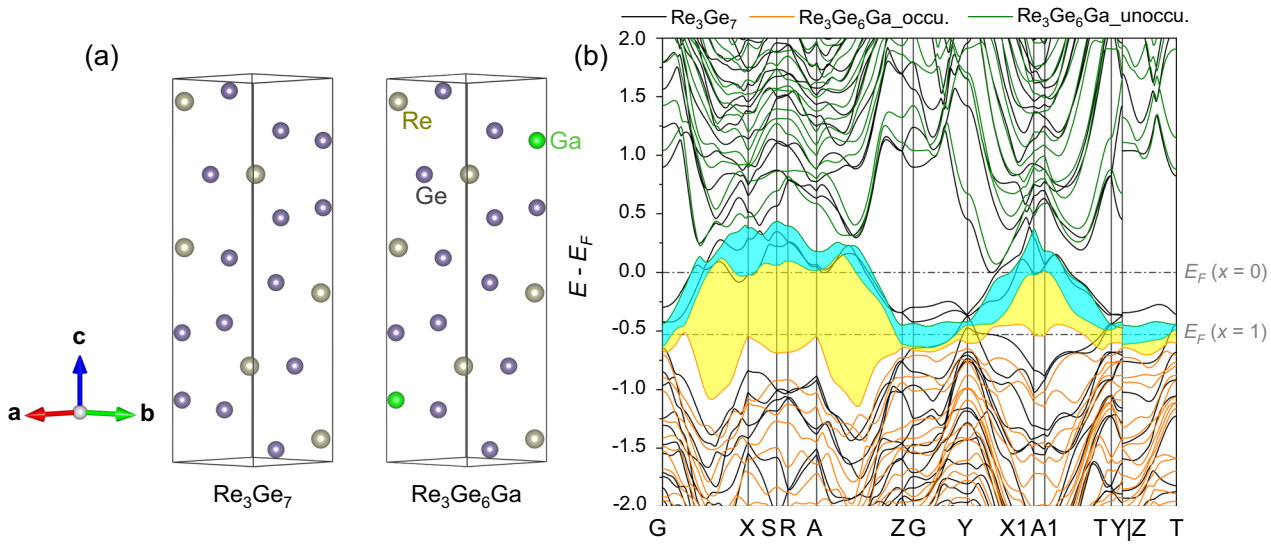

Fig. 7 Hypothetical crystal structure and corresponding electronic structure of Re_3Ge_6Ga. a The primitive cell for Re_3Ge_7 and a possible *C*2/*m* configuration of Re_3Ge_6Ga. **b** Bulk band structure for Re_3Ge_6Ga with space group *C*2/*m*. The cyan and yellow regions correspond to the band filling of $x = 0$ and 1, respectively.

spectroscopy measurements on the superconducting gap symmetry and possible in-gap states.

In summary, we have discovered SC in the orthorhombic $Re_3Ge_{7-x}Ga_x$ system. The pristine Re_3Ge_7 exhibits a second order metal–insulator-like phase transition below 57.3 K, which is suppressed upon Ga doping and disappears above $x = 0.2$. At this doping level, SC starts to be observed and T_c displays a dome-like dependence with a maximum value of 3.37 K at $x = 0.25$. The Hall effect measurements indicate that substitution of Ga for Ge introduces holes, consistent with the band structure calculations. The theoretical results further suggest that the phase transition in Re_3Ge_7 is likely driven by Fermi-surface nesting and superconducting $Re_3Ge_{7-x}Ga_x$ compositions exhibit nontrivial band topology characterized by strong Z_2 invariants. Our results indicate that Ga-doped Re_3Ge_7 is a rare system that combines collective phase transition, nontrivial band topology and SC, which lays a foundation for further exploring the competition and interplay between these properties.

METHODS

Sample synthesis

Polycrystalline $Re_3Ge_{7-x}Ga_x$ samples with $x = 0$, 0.1, 0.2, 0.25, 0.3, 0.35, and 0.4 were prepared by the solid-state reaction method. High-purity Re (99.99%), Ge (99.99%) powders, and Ga (99.999%) shots were weighed according to the stoichiometric ratio, mixed thoroughly and pressed into pellets in an argon-filled glove box. The pellets were then sealed in evacuated silica tubes and heated at 850 °C for several days, followed by slow cooling to room temperature. This process was repeated several times with intermediate grindings to ensure homogeneity.

Structural characterizations

The phase purity of resulting samples was examined by powder XRD using a Bruker D8 Advance X-ray diffractometer with Cu Kα radiation. The data were collected with a step-scan mode in the 2θ range from 5° to 120° and the structural refinements were performed using the program JANA2006[34].

Physical property measurements

Measurements of resistivity, Hall coefficient and specific heat were done on regular-shaped samples in a Quantum Design Physical Property Measurement System (PPMS-9 Dynacool). The resistivity was measured by the four-probe method and down to 150 mK at zero field using an adiabatic dilution refrigerator option. The Hall resistivity was measured by sweeping the field from −9 to 9 T, and the data were antisymmetrized to remove the magnetoresistance contribution. The zero-field cooling and field cooling magnetic susceptibility measurements down to 0.4 K were carried out using a Quantum Design Magnetic Property Measurement System (MPMS3).

Theoretical calculations

Our first principles calculations were performed within density functional theory, as implemented in the Vienna Ab-initio Simulation Package[35]. The Kohn–Sham equations were constructed on a projector augmented wave basis[36]. The exchange-correlation energy was calculated with a Perdew–Burke–Ernzerhof type functional[37]. For all calculations, we adopted a monoclinic primitive cell with experimental lattice parameters. The plane-wave energy cutoff for wavefunctions was set to 600 eV. The ***k***-mesh was set $12 \times 12 \times 3$ for self-consistent calculations and $24 \times 24 \times 6$ for DOS calculations. To calculate the band dispersion over the whole Brillouin zone more efficiently, we constructed a tight-binding Hamiltonian with maximally localized Wannier functions[38]. The Fermi surfaces and nesting functions were then calculated with this tight-binding Hamiltonian.

DATA AVAILABILITY

The data that support the findings of this study are available from the corresponding author upon reasonable request.

Received: 31 December 2020; Accepted: 15 July 2021;
Published online: 13 August 2021

REFERENCES

1. Bednorz, J. G. & Muller, K. A. Possilbe high T_c superconductivity in the Ba-La-Cu-O system. *Z. Phys. B* **64**, 189–193 (1986).
2. Jaccard, D., Behnia, K. & Sierro, J. Pressure induced heavy fermion superconductivity of $CeCu_2Ge_2$. *Phys. Lett. A* **163**, 475–480 (1992).
3. Morosan, E. et al. Superconductivity in Cu_xTiSe_2. *Nat. Phys.* **2**, 544–550 (2006).
4. Kamihara, Y., Watanabe, T., Hirano, M. & Hosono, H. Iron-based layered superconductor $La[O_{1-x}F_x]FeAs$ ($x = 0.05$-0.12) with $T_c = 26$ K. *J. Am. Chem. Soc.* **130**, 3296–3297 (2008).
5. Budnick, J. I. et al. Observation of magnetic ordering in La_2CuO_4 by moun spin rotation spectroscopy. *Phys. Lett. A* **124**, 103–106 (1987).
6. de Boer, F. R. et al. $CeCu_2Ge_2$: Magnetic order in a Kondo lattice. *J. Magn. Magn. Mater.* **63**, 91–94 (1987).
7. de la Cruz, C. et al. Magnetic order close to superconductivity in the iron-based layered $LaO_{1-x}F_xFeAs$ systems. *Nature* **453**, 899–902 (2008).

8. Di Salvo, F. J., Moncton, D. E. & Waszczak, J. V. Electronic properties and superlattice formation in the semimetal $TiSe_2$. *Phys. Rev. B* **14**, 4321–4328 (1976).
9. McGuire, M. A. et al. Phase transitions in LaFeAsO: Structural, magnetic, elastic, and transport properties, heat capacity and Mossbauer spectra. *Phys. Rev. B* **78**, 094517 (2008).
10. Campbell, D. J. et al. Intrinsic insulating ground state in transition metal dichalcogenide $TiSe_2$. *Phys. Rev. Mater.* **3**, 053402 (2019).
11. Qi, X. L. & Zhang, S. C. Topological insulators and superconductors. *Rev. Mod. Phys.* **83**, 1057–1110 (2011).
12. Alicea, J. New directions in the pursuit of Majorana fermions in solid state systems. *Rep. Prog. Phys.* **75**, 076501 (2012).
13. Sato, M. & Ando, Y. Topological superconductors: a review. *Rep. Prog. Phys.* **80**, 076501 (2017).
14. Hor, Y. S. et al. Superconductivity in $Cu_xBi_2Se_3$ and its implications for pairing in the undoped topological insulator. *Phys. Rev. Lett.* **104**, 057001 (2010).
15. Sasaki, S. et al. Odd-parity pairing and topological superconductivity in a strongly spin-orbit coupled semiconductor. *Phys. Rev. Lett.* **109**, 217004 (2012).
16. Liu, Z. H. et al. Superconductivity with topological surface state in $Sr_xBi_2Se_3$. *J. Am. Chem. Soc.* **137**, 10512–10515 (2015).
17. Wang, Z. W. et al. Superconductivity in $Tl_{0.6}Bi_2Te_3$ derived from a topological insulator. *Chem. Mater.* **28**, 779–784 (2016).
18. Asaba, T. et al. Rotational symmetry breaking in a trigonal superconductor Nb-doped Bi_2Se_3. *Phys. Rev. X* **7**, 011009 (2017).
19. Zhu, L. et al. Superconductivity in potassium-intercalated T_d-WTe_2. *Nano Lett.* **18**, 6585–6590 (2018).
20. Wu, J. F. et al. Doping-induced superconductivity in the topological semimetal Mo_5Si_3. *Chem. Mater.* **32**, 8930–8937 (2020).
21. Siegrist, T., Hulliger, F. & Petter, W. The crystal sructure of Re_3Ge_7. *J. Less Common Met.* **90**, 143–151 (1983).
22. Rabus, A. & Mun, E. Anomalous transport properties of Re_3Ge_7. *Phys. Rev. Mater.* **3**, 013404 (2019).
23. Zhang, T. T. et al. Catalogue of topological electronic materials. *Nature* **566**, 475–479 (2019).
24. Tarutani, Y. & Kudo, M. Atomic radii and lattice parameters of the A15 crystal structure. *J. Less Common Met.* **55**, 221–229 (1977).
25. Kittel, C. *Introduction to Solid State Physics* (John Wiley, 1996).
26. Stewart, G. R. Superconductivity in iron compounds. *Rev. Mod. Phys.* **83**, 1589–1652 (2011).
27. Bardeen, J., Cooper, L. N. & Schreiffer, J. R. Theory of superconductivity. *Phys. Rev.* **108**, 1175–1204 (1957).
28. Young, S. M. et al. Dirac semimetal in three dimensions. *Phys. Rev. Lett.* **108**, 140405 (2012).
29. Gao, H., Venderbos, J. W. F., Kim, Y. & Rappe, A. M. Topological semimetal from first-principles. *Annu. Rev. Mater. Res.* **49**, 153–183 (2019).
30. Landa, A. et al. Fermi surface nesting and pre-martensitic softening in V and Nb at high pressures. *J. Phys.: Condens. Matter* **18**, 5079–5085 (2006).
31. Errea, I., Martinez-Canales, M., Oganov, A. R. & Bergara, A. Fermi surface nesting and phonon instabilities in simple cubic calcium. *High. Press. Res.* **28**, 443–448 (2008).
32. Fu, L., Kane, C. L. & Mele, E. J. Topological insulators in three dimensions. *Phys. Rev. Lett.* **98**, 106803 (2007).
33. Fu, L. & Kane, C. L. Topological insulators with inversion symmetry. *Phys. Rev. B.* **76**, 045302 (2007).
34. Petricek, V., Dusek, M. & Palatinus, L. Crystallographic computing system JANA2006: General features. *Z. Kristallogr.* **229**, 345–352 (2014).
35. Kresse, G. & Hafner, J. Ab initio molecular dynamics for liquid metals. *Phys. Rev. B* **47**, 558(R) (1993).
36. Blochl, P. E. Projector augmented-wave method. *Phys. Rev. B* **50**, 17953 (1994).
37. Perdew, J. P., Burke, K. & Ernzerhof, M. Generalized gradient approximation made simple. *Phys. Rev. Lett.* **77**, 3865–3868 (1996).
38. Marzari, N. & Vanderbilt, D. Maximally localized generalized Wannier functions for composition energy bands. *Phys. Rev. B* **56**, 12847–12865 (1997).

ACKNOWLEDGEMENTS

We acknowledge financial support by the foundation of Westlake University and National Key Research Development Program of China (No. 2017YFA0303002).

AUTHOR CONTRIBUTIONS

Y.W.C. and Z.R. conceived the project. Y.W.C. synthesized the samples and did the physical property measurements with the assistance from Q.Q.Z., G.X.X., B.L. and J.F. W. S.Q.W. and G.H.C. performed theoretical calculations. Z.R. supervised the project and wrote the paper with inputs from Y.W.C. and S.Q.W.

COMPETING INTERESTS

The authors declare no competing interests.

ADDITIONAL INFORMATION

Supplementary information The online version contains supplementary material available at https://doi.org/10.1038/s41535-021-00372-z.

Correspondence and requests for materials should be addressed to Z.R.

Reprints and permission information is available at http://www.nature.com/reprints

Publisher's note Springer Nature remains neutral with regard to jurisdictional claims in published maps and institutional affiliations.